Interaction of Kelvin force and transport across a melting substrate in a microgravity environment

Nicholas K. Burgess* and Kannan N. Premnath†
Department of Mechanical Engineering, University of Wyoming, Laramie, Wyoming 82071, USA
(Received 8 June 2010; revised manuscript received 31 August 2010; published 8 October 2010)

Gradients in magnetic field applied to electrically insulating fluids result in an effective body force—the Kelvin force, which can potentially be used to control flow and thermal processes, particularly in microgravity environments. We study the influence of the Kelvin force on the mass, momentum, and energy transport of fluid arising from the melting of a semi-infinite solid substrate subjected to temperature and magnetic-field gradients. The governing equations of the magnetothermal free convection of the melt under the boundary layer approximation with a suitable transformation lead to a similarity solution. Closed-form analytical solutions for the limiting case of smaller Prandtl numbers are presented. The nonlinear similarity equations are solved numerically using an iterative boundary-value technique based on a finite-difference approach. Based on the numerical results, the effect of various characteristic nondimensional parameters on the structure of the melt boundary layer and transport rates of heat and mass across the substrate are elucidated and discussed.

DOI: 10.1103/PhysRevE.82.046303 PACS number(s): 44.20.+b, 44.05.+e, 44.25.+f, 68.08.−p

I. INTRODUCTION

When an electrically insulating fluid is subjected to nonuniform magnetic fields, it induces the Kelvin force, a volumetric force, on the fluid. The magnitude and direction of this force depend on the magnetic susceptibility of the material, the strength of the applied magnetic field, and its gradient [1]. By using magnets of sufficient strengths, this force can be made to align with the center of mass of the fluid in a parallel or antiparallel manner to create artificial variable gravity-like environments. In contrast to the Lorentz force in magnetohydrodynamics, which arise from the interaction of the magnetic field with the flow of an electrically conducting fluid [2], the Kelvin force results from the microscopic alignment of dipole moments due to magnetic-field gradients [1]. As a result, the latter can have an influence on all types of insulating fluids—both paramagnetic and diamagnetic. Specifically, regions of higher magnetic-field strength result in an attractive Kelvin force for paramagnetic fluids, while becoming repulsive for diamagnetic substances [3]. One important potential application of this force lies in the design and control of thermal and material transport processes in such situations where the terrestrial gravity effects are negligible, including material processing applications in spacecraft, where the effect of Kelvin force can become particularly pronounced.

Beaugnon and Tournier [4], in a seminal work, provided a successful experimental demonstration of the levitation of ordinary diamagnetic liquids, such as water, ethanol, and acetone in the presence of an applied magnetic-field gradient, i.e., Kelvin force. On the other hand, the same group also investigated the combined effect of an applied thermal and magnetic-field gradient inducing magnetothermal free convection at around the same time [5]. It may be noted that one of the earliest studies in this regard was carried out by Carruthers and Wolfe [6]. They showed that the buoyancy effects induced by the Kelvin force can even exceed that of gravitational buoyancy on convection in a rectangular chamber for terrestrial conditions with appropriate magnitude of the magnetic-field gradients. An analytical solution for fully developed convection between parallel plates by including the magnetic and thermal gradient effects was obtained later [7]. In a series of articles, Huang *et al.* [8–10] studied convective instability of a layer of paramagnetic fluid heated from below and subjected to Kelvin force effects, which was also extended to diamagnetic fluids [11]. It may be noted that similar studies have been carried out for the case of artificial ferrofluids starting from the work of Finlayson [12–14]. A detailed theoretical analysis of the magnetothermal convection was also carried out by Bai *et al.* [15]. Wakayama *et al.* [16] provided an effective vertical acceleration control method that can vary continuously from normal gravity to close to zero gravity using Kelvin forces, proving the concept by means of an experimental investigation. Gray *et al.* [3] studied magnetothermal plumes by means of a similarity solution based on a boundary layer analysis. They also demonstrated that Kelvin forces can be treated as a buoyancy-type force for such problems in a similar way to gravity but in a generalized sense with a spatially variable acceleration term. Akamatsu *et al.* [17] showed that magnetothermal gradients can lead to the formation of jet flow by means of a numerical study. Experimental measurement studies of the enhancement of natural convection in cubical enclosures by means of Kelvin force were carried out by Bednarz *et al.* [18]. Recently, Larachi and Munteanu [19] experimentally studied the influence of gradients in magnetic fields on the hydrodynamic properties of electrically insulating two-phase (gas-liquid) flows.

An interesting possibility with potential applications is the use of Kelvin force to control phase-change processes in electrically insulating materials, such as melting or solidification in the presence of thermal gradients by means of suitable magnetic field gradients. In fact, the early work by Carruthers and Wolfe [6] suggests this application for crystal-

*nburges2@uwyo.edu
†knandhap@uwyo.edu

growth control of certain diamagnetic liquids by analyzing data based on a contemporary measurement [20]. More recently, in a related context, Wakayama *et al.* [21] performed visualization studies of the influence of Kelvin force on protein crystal formation. It was found that when the Kelvin force applied to a supersaturated protein solution is effectively upward (downward), then the protein crystals were found to be improved (deteriorated) [22]. Furthermore, Tagami *et al.* [23] demonstrated the solidification of levitating water droplet by means of Kelvin force using an experimental setup in a microgravity environment. Recent studies in this direction include the work by Ramachandran and Leslie [24].

Phase-change problems involving melting or solidification have numerous applications related to material processing. A canonical problem in this regard is the melting of a semi-infinite substrate—the Stefan problem [25]—is rich in nonlinear physics representing coupled transport phenomena with moving interfaces. In the context of electrically conducting materials, the Lorentz force induced by magnetic field has been used to control a number of materials processing applications, such as crystal growth, semiconductor fabrication, and casting of steel [26–28]. In particular, Seeniraj and Kannan [29] investigated the effect of the Lorentz force on the melting transport by means of an integral analysis approach. On the other hand, a theoretical or numerical study of the effect of Kelvin force on the phase-change processes in microgravity environments, where it has particular significance with potential applications, is desired.

Thus, the focus of this work is on the theoretical and numerical investigation of the influence of Kelvin forces on the transport for the following configuration of a melting substrate. We consider a semi-infinite block of insulating material (paramagnetic or diamagnetic) subjected to thermal and magnetic-field gradients. The presence of thermal gradients causes steady heat transfer into the solid resulting in phase change to fluid as the latent heat of phase transformation as well as the heat capacity due to its initial subcooling is overcome. It may be noted that in the absence of convection, heat propagation by pure conduction only causes smoothening of temperature profile, with no regime of moving melting front of stationary profile. On the other hand, convection in melted phase provides additional intense heat influx to the melting front that cannot be balanced by a purely conductive heat influx into the solid phase. This unbalanced energy influx goes into the latent heat of melting in such a way that any buoyant convection in liquid phase unavoidably leads to propagation of the melting front into the solid phase. Such propagation can be associated with stationary profile solution, as considered in this work.

By assuming the Boussinesq approximation for the density as well as the magnetic susceptibility, the Kelvin force is rewritten as a buoyancy force with a magnetic acceleration term that drives the magnetothermal convection of the liquid melt. The two-dimensional (2D) coupled mass, momentum, and energy equations of the melt are simplified by means of the standard boundary layer approximation [30]. To facilitate the analysis, the phase boundary is immobilized by means of a variable transformation first suggested by Landau [31] and extended by others [32–34]. As a result, the mass and energy

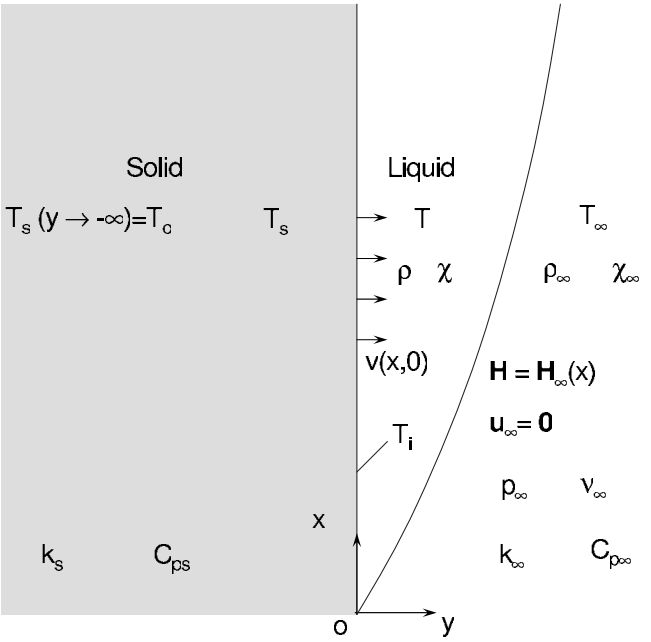

FIG. 1. Schematic arrangement of the physical configuration.

transport across the phase boundary controlled by the Kelvin force appears as a boundary condition to the boundary layer equations for the melt. Under a suitable choice of power-law variations for the Kelvin force, it will be shown that the governing equations and the attendant boundary conditions exhibit similarity, which are solved by means of a nonlinear finite-difference technique. Here, we consider vicinity of singularities of the magnetic fields and the phrase "power law" mentioned here and henceforth refer to the order of singularity. This allows investigation of the effect of the various characteristic parameters, including different power laws for the Kelvin force, on the melt free convection flow and temperature distribution, as well the transport rates across the phase boundary.

The paper is organized as follows: Section II discusses the theoretical formulation of the mass, momentum, and energy transport of the melt with attendant phase-change boundary conditions in the presence of the Kelvin force. It also presents the resulting simplification as a similarity solution due to the boundary layer approximation. Section III discusses the asymptotic solution for small Prandtl numbers based on this similarity formulation. The numerical solution procedure employed is presented in Sec. IV. Section V provides the numerical results and discusses the influence of various governing parameters. Finally, summary and conclusions of this paper are presented in Sec. VI.

II. GOVERNING EQUATIONS

A schematic of the physical configuration consisting of the magnetothermal free convection of an electrically insulating (paramagnetic or diamagnetic) liquid layer resulting from the melting of semi-infinite solid substrate subjected to thermal and magnetic-field gradients is illustrated in Fig. 1. The equations governing the motion of the melt fluid are the

steady, incompressible Navier-Stokes equations under an extended Bousinessq approximation for fluid properties given by

$$\nabla \cdot \mathbf{u} = \mathbf{0}, \tag{1}$$

$$\rho_\infty \mathbf{u} \nabla \cdot \mathbf{u} = -\nabla p - \rho \mathbf{g} + \rho_\infty \nu_\infty \nabla^2 \mathbf{u} + \mu_0 \frac{\chi}{2} \nabla (\mathbf{H}^2), \tag{2}$$

where the last term in Eq. (2) is the Kelvin force due to the applied magnetic field $\mathbf{H}$ [1]. Here, both the properties, viz., the density ρ and the magnetic susceptibility χ, are allowed to vary only for the terms involving the gravity and Kelvin body forces, respectively—hence the characterization as the extended Bousinessq approximation. μ_0 is the permeability of free space and ν is the kinematic viscosity of the fluid. The subscript "∞" refers to the static conditions, i.e., those that are at far distances from the substrate-liquid phase boundary. For the 2D flow under consideration the velocity vector is $\mathbf{u}=(u,v)^\dagger$, where "†" is the transpose. The equation governing the temperature distribution in the melt is the conservation of energy for the incompressible melt flow given as

$$\rho_\infty C_{p_\infty} \mathbf{u} \cdot \nabla T = k_\infty \nabla^2 T, \tag{3}$$

where C_{p_∞} and k_∞ are the specific heat at constant pressure and thermal conductivity, respectively, of the liquid. Here, as in [3], the effect of magnetic terms in Eq. (3) is neglected.

For the 2D flow under consideration the following boundary conditions for the fluid variables are given by

$$u(x,0) = 0,$$

$$u(x,\infty) = u_\infty = 0,$$

$$v(x,0) = v_i(x,0),$$

$$T(x,0) = T_i,$$

$$T(x,\infty) = T_\infty, \tag{4}$$

where T_i is the specified "melting" temperature and $v_i(x,0)$ is the normal velocity (unknown *a priori*) at the substrate-melt layer interface.

The magnetic field satisfies a simplified form of Maxwell's equations given as

$$\nabla \cdot \mathbf{B} = \mathbf{0}, \quad \nabla \times \mathbf{H} = \mathbf{0}, \quad \mathbf{B} = \mu_\mathbf{0}(\mathbf{1} + \chi)\mathbf{H}.$$

Thus,

$$\nabla \cdot \mathbf{H} \approx \mathbf{0}. \tag{5}$$

This particular form implies that the magnetic field is unaffected by the flow and hence we are free to specify a magnetic field $\mathbf{H}=\mathbf{H}_\infty$. Further, there is no need to explicitly solve Maxwell's equations along with the equations of fluid motion and energy transport.

The equation governing the melting of the solid substrate is the steady heat conduction equation with its interface front with the liquid moving with an as yet unknown velocity $v_s(x,0)$. Note that the conservation of mass at the interface implies $\rho_s v_s(x,0)=\rho v(x,0)$. This expression is valid for the reference frame fixed to the melting front, as considered in the following. The essential physical element here is that the heat supplied to the substrate at the interface should overcome the latent heat of melting $\mathcal{L}$ and the heat capacity of the substrate if it is at a subcooled temperature T_o (i.e., $T_o < T_i$) as the front maintains a steady local melting velocity. By means of a suitable transformation applied to this governing equation, first suggested by Landau, the boundary can be effectively immobilized [31–33], and, ultimately, the influence of the physical processes in the solid appears as a boundary condition for the liquid melt. Thus, the effective nondimensional heat conduction for the solid substrate is written as [29,34]

$$\frac{d^2\theta_s}{d\bar{y}^2} - \kappa\lambda \frac{\mathrm{Ste}_f}{\mathrm{Ste}_s} \frac{v(x,0)}{\sigma_f} \frac{d\theta_s}{d\bar{y}} = 0,$$

$$\theta_s(\bar{y}=0) = 1, \quad \theta_s(\bar{y} \to -\infty) = 0, \tag{6}$$

where the various dimensionless groups are given by

$$\bar{y} = \frac{y}{l}, \quad \theta_s = \frac{T_s - T_o}{T_i - T_o}, \quad \lambda = \frac{T_\infty - T_i}{T_i - T_o}, \quad \kappa = \frac{k_\infty}{k_s},$$

$$\sigma_f = \frac{k_\infty}{\rho_\infty C_{p_\infty}}, \quad \mathrm{Ste}_f = \frac{C_{p_\infty}(T_\infty - T_i)}{\mathcal{L}}, \quad \mathrm{Ste}_s = \frac{C_{p_s}(T_i - T_o)}{\mathcal{L}}.$$

Here, l is a characteristic length and T_o and T_∞ are the temperatures at far off distance from the interface in the solid and liquid, respectively. λ is the ratio of the degree of superheating in the liquid melt to the degree of subcooling in the substrate, κ is the ratio of thermal conductivities of the liquid to the solid, and σ_f is the thermal diffusivity of the liquid; furthermore, an important characteristic dimensionless group for phase-change problems is the Stefan number (Ste), which represents the ratio of the heat capacity of a given phase to the latent heat of phase change (melting). Here, Ste_f and Ste_s are the Stefan numbers for the liquid and solid phases, respectively. The governing equation for the substrate can be readily solved to yield [29]

$$\theta_s = \exp\left[\kappa\lambda \frac{\mathrm{Ste}_f}{\mathrm{Ste}_s} \frac{v_s(x,0)l}{\sigma_f} \bar{y}\right]. \tag{7}$$

Using this solution the condition for the rate of heat transfer to the liquid melt can be evaluated as follows:

$$k_\infty \left.\frac{\partial T}{\partial y}\right|_{y=0^+} = \rho_s \mathcal{L} v_s(x,0) + k_s \left.\frac{\partial T_s}{\partial y}\right|_{y=0^-}, \tag{8}$$

in which when Eq. (7) is used for the substrate temperature distribution yields

$$k_f \left.\frac{\partial T}{\partial y}\right|_{y=0^+} = \rho_s \mathcal{L} v_s(x,0) + c_{p_s} \rho_s v_s(x,0)(T_i - T_o). \tag{9}$$

Thus, this finally gives an effective coupled boundary condition between the normal velocity $v(x,0)$ and the rate of heat transfer at the interface front for use with the liquid melt layer transport equations.

To proceed further, let us now evaluate the momentum equation [Eq. (2)] of the melt at far off distances from the interface giving

$$0 = -\rho_\infty \mathbf{g} - \nabla p_\infty + \mu_0 \frac{\chi_\infty}{2} \nabla \mathbf{H}^2, \tag{10}$$

which essentially is a restatement of the force balance under static conditions. Subtracting this from the full momentum equation [Eq. (2)] results in

$$\rho_\infty \mathbf{u} \nabla \cdot \mathbf{u} = -\nabla(p - p_\infty) + (\rho - \rho_\infty)\mathbf{g} + \rho_\infty \nu_\infty \nabla^2 \mathbf{u} + \frac{\mu_0}{2}(\chi - \chi_\infty) \nabla (\mathbf{H}^2). \tag{11}$$

Using the standard Boussinesq approximation for the density by means of the temperature excess $(T_\infty - T)$,

$$\rho = \rho_\infty [1 - \alpha_\infty (T_\infty - T)] \tag{12}$$

gives a coupling between the momentum and energy equations of the motion of the melt. Here, α_∞ is the coefficient of thermal expansion $(\alpha_\infty > 0)$.

A. Kelvin force as a buoyancy force

The Kelvin force can also be characterized as a buoyancy force through some manipulation [3]. To cast the Kelvin force as a buoyancy force, the susceptibility χ which is, in general, both a function of density and temperature $[\chi(T,\rho)]$ is expanded in a Taylor series as

$$\chi(T,\rho) = \chi_\infty + \left.\frac{\partial \chi}{\partial T}\right|_\infty (T - T_\infty) + \left.\frac{\partial \chi}{\partial \rho}\right|_\infty (\rho - \rho_\infty) + O(\Delta T^2, \Delta \rho^2), \tag{13}$$

where $\Delta T = T - T_\infty$ and $\Delta \rho = \rho - \rho_\infty$. For small temperature variations, the series is truncated to first order (dropping the higher order terms in the above expansion). In particular, considering that paramagnetic substances obey Curie's law (i.e., $\chi = C\rho/T$), while the diamagnetic fluids satisfy $\chi = \chi_m \rho$, and taking $\frac{\partial \chi}{\partial \rho}|_\infty = \chi_\infty / \rho_\infty$, we can write a unified variation for susceptibility under the above extended Bousinessq approximation [3],

$$\chi = \chi_\infty - \frac{\chi_\infty}{\rho_\infty} \alpha_\infty \beta_\infty (T_\infty - T), \tag{14}$$

where $\beta_\infty = 1 - 1/\alpha_\infty T_\infty$ and $\beta_\infty = 1$ for paramagnetic and diamagnetic fluids, respectively. As a result, the Kelvin force, in terms of the local temperature excess, magnetic-field gradient, and other parameters, can now be rewritten as

$$\mathbf{F}_k = \mu_0 \frac{(\chi - \chi_\infty)}{2} \nabla \mathbf{H}^2 = -\frac{\mu_0}{2} \chi_\infty \alpha_\infty \beta_\infty (T_\infty - T) \nabla \mathbf{H}^2. \tag{15}$$

This force, which may be characterized as a "Kelvin buoyancy force" as it also leads to a coupling of momentum and energy transport, can be conveniently presented in terms of a generalized magnetic acceleration term as

$$\mathbf{F}_k = -\rho_\infty \alpha_\infty (T_\infty - T)\mathbf{g}_k, \tag{16}$$

where

$$\mathbf{g}_k = \frac{\mu_0}{2} \frac{\chi_\infty}{\rho_\infty} \beta_\infty \nabla \mathbf{H}^2. \tag{17}$$

Note that given the sign of Eq. (16), the spatially dependent "gravity-like" term arising due to magnetic-field gradient $\mathbf{g}_k$ in Eq. (17) will induce "buoyancy" fluid motion provided it has a negative sign. Thus, Eq. (11), using Eqs. (12), (16), and (17), can finally be written analogously to the classical free convection with the addition of a magnetic acceleration term $\mathbf{g}_k$, leading to the so-called magnetothermal momentum equation of the melt layer as

$$\rho_\infty \mathbf{u} \nabla \cdot \mathbf{u} = -\nabla(p - p_\infty) - \rho_\infty \alpha_\infty (T_\infty - T)(\mathbf{g} + \mathbf{g}_k) + \rho_\infty \nu_\infty \nabla^2 \mathbf{u}. \tag{18}$$

The final form of the governing equations is given in Eqs. (1), (3), and (18) with boundary conditions given in Eqs. (4) and (9), which will be used to derive boundary layer and corresponding similarity equations. Note that the Kelvin force is proportional to the gradient of the magnetic-field magnitude squared.

B. Microgravity boundary layer

A microgravity environment is one in which the acceleration due to gravity is considered negligible $(\mathbf{g} \approx 0)$, in which case the Kelvin buoyancy force assumes particular significance and can be used to appropriately control melting heat transfer rates. Further in this analysis there will be no free stream velocity and the free stream pressure and temperature will be assumed constant. The standard order-of-magnitude arguments (e.g., [3]) are used to simplify the equations governing the melt to give boundary layer equations as

$$\frac{\partial u}{\partial x} + \frac{\partial v}{\partial y} = 0, \tag{19}$$

$$u\frac{\partial u}{\partial x} + v\frac{\partial u}{\partial y} = -\alpha_\infty (T_\infty - T)\mathbf{g}_k + \nu_\infty \frac{\partial^2 u}{\partial y^2}, \tag{20}$$

$$u\frac{\partial T}{\partial x} + v\frac{\partial T}{\partial y} = \sigma_\infty \frac{\partial^2 T}{\partial y^2}. \tag{21}$$

These boundary layer equations are subjected to the boundary conditions given in Eqs. (4) and (9).

C. Similarity solution

Introducing a stream function (ψ) that automatically satisfies the conservation of mass by requiring

$$u = \frac{\partial \psi}{\partial y}, \quad v = -\frac{\partial \psi}{\partial x},$$

a similarity solution for the stream function is sought. The similarity variables are defined by

$$\eta = \frac{ay}{x^r}, \quad \psi = G(x) f(\eta), \quad G(x) = bx^{\xi},$$

with additional similarity variables for the temperature and applied Kelvin buoyancy force given by

$$\theta(\eta) = \frac{T - T_i}{T_\infty - T_i},$$

$$g_k(x) = -Mx^{\phi}, \tag{22}$$

where a, b, r, ϕ, M, and ξ are constants. Here, $M > 0$ and a negative sign is used for g_k to be consistent with the requirement for inducing fluid motion due to buoyancy effects as discussed in Sec. II B. Introducing these into Eqs. (20) and (21) and using the definitions of velocities in terms of the stream function one arrives (after lengthy simplification) at the following equation governing the similarity variable f as

$$(\xi - r)(f')^2 - \xi f f'' = -\alpha_\infty (T_\infty - T_i) M(\theta - 1) \frac{x^{\phi}}{a^2 b^2 x^{2(\xi - r) - 1}} + \frac{\nu_\infty a^3 b}{a^2 b^2} \frac{x^{\xi - 3r}}{x^{2(\xi - r) - 1}} f''', \tag{23}$$

In order to obtain a similarity solution it is required that all coefficients be independent of the x coordinate, giving the following constraint equations $-(\xi + r) + 1 = 0 \Rightarrow r = (1 - \xi)$ and $\phi - 2(\xi - r) + 1 = 0 \Rightarrow \xi = (\phi + 3)/4$, the solution of which gives relations between r and ξ and the Kelvin force parameter ϕ as $r = \frac{1}{4}(1 - \phi)$ and $\xi = \frac{1}{4}(\phi + 3)$. Substitution of these into Eq. (23) yields

$$2(\phi + 1)(f')^2 - (\phi + 3) f f'' = -\frac{4\alpha_\infty}{a^2 b^2} (T_\infty - T_i) M(\theta - 1) + 4\nu_\infty \frac{a}{b} f''', \tag{24}$$

For further simplification, we set $4\alpha_\infty (T_\infty - T_i) M / a^2 b^2 = 1$ and $4\nu_\infty \frac{a}{b} = 1$, and solving gives

$$a = \left[\frac{M \alpha_\infty (T_\infty - T_i)}{4\nu_\infty^2} \right]^{1/4}, \quad b = 4\nu_\infty a,$$

thus yielding the final equation for the similarity variable f as

$$f''' + (\phi + 3) f f'' - 2(\phi + 1)(f')^2 - (\theta - 1) = 0. \tag{25}$$

Using an analogous procedure for the energy equation gives

$$\theta'' + \mathrm{Pr}(\phi + 3) f \theta' = 0, \tag{26}$$

where Pr is the Prandtl number given by $\mathrm{Pr} = \nu_\infty / \sigma_\infty$. The boundary conditions for the similarity equations are obtained from Eqs. (4) and (9) as

$$f'(0) = 0, \quad f'(\infty) = 0, \quad \theta(0) = 0, \quad \theta(\infty) = 1,$$

$$B\theta'(0) + (\phi + 3)\mathrm{Pr} f(0) = 0, \tag{27}$$

where B is referred to as the melting parameter, as it characterizes the melting effects in terms of dimensionless groups and is given by

$$B = \frac{C_{p_\infty} (T_\infty - T_i)}{\mathcal{L} + C_{p_s} (T_i - T_o)} = \frac{\mathrm{Ste}_f}{1 + \mathrm{Ste}_s}.$$

The solution of Eqs. (25) and (26) together with the boundary conditions in Eq. (27) gives all the information required to compute velocity and temperature profiles as well as melting and heat transfer rates in the liquid melt layer. In particular, in this regard, the components of the velocity field can be rewritten in terms of new dimensionless groups by defining the local magnetic Grashoff number from parameter a as

$$\mathrm{Gr}_{M,x} = \frac{M \alpha_\infty (T_\infty - T_i) x^3}{\nu_\infty^2}.$$

The similarity variables then reduce to

$$\eta = \left(\frac{\mathrm{Gr}_{M,x}}{4} \right)^{1/4} \frac{y}{x^{1 - \phi/4}}, \quad \psi = 4\nu_\infty \left(\frac{\mathrm{Gr}_{M,x}}{4} \right)^{1/4} x^{\phi/4} f(\eta).$$

Furthermore, defining the characteristic velocity U_o based on the parameters a and b for the problem involving thermal and magnetic-field gradients as

$$U_o = 2[M \alpha_\infty (T_\infty - T_i)]^{1/2} x^{(\phi + 1)/2},$$

we can finally write

$$\frac{u}{U_o} = f'(\eta),$$

$$\frac{v}{U_o} = -\frac{1}{4} \left(\frac{\mathrm{Gr}_{M,x}}{4} \right)^{-1/4} x^{-\phi/4} [(\phi + 3) f(\eta) - (1 - \phi) \eta f'].$$

In addition, the local heat transfer coefficient may now be written as

$$h_x = \frac{k \left(\frac{\partial T}{\partial y} \right)_{y=0}}{(T_\infty - T_i)} = k \left(\frac{\partial \theta}{\partial y} \right)_{y=0} = \frac{k}{x^{1 - \phi/4}} \left(\frac{\mathrm{Gr}_{M,x}}{4} \right)^{1/4} \theta'(0),$$

which yields the local Nusselt number as

$$\mathrm{Nu}_x = \frac{h_x x}{k} = x^{\phi/4} \left(\frac{\mathrm{Gr}_{M,x}}{4} \right)^{1/4} \theta'(0),$$

which provides a nondimensional characterization of the heat transfer rate at the melt interface front. Based on this, we arrive at the nondimensional local melting rate as

$$\frac{v(x,0) x}{\sigma_\infty} = B \mathrm{Nu}_x.$$

Finally, the power-law parameter ϕ can be related to the applied magnetic-field strength $H(x)$ using the definition of the magnetic acceleration term and Kelvin buoyancy force as $H(x) = H_o x^{(\phi + 1)/2}$ for $\phi \neq -1$ and $H(x) = H(x_{min}) [\ln(x / x_{min})]^{1/2}$ for $\phi = -1$, where $x > x_{min} > 0$. Note that both $U_o = U_o(x)$ and $H(x)$ follow similar power-law variations. This yields the following expressions for the proportionality parameter M in the magnetic acceleration term in terms of all known variables as

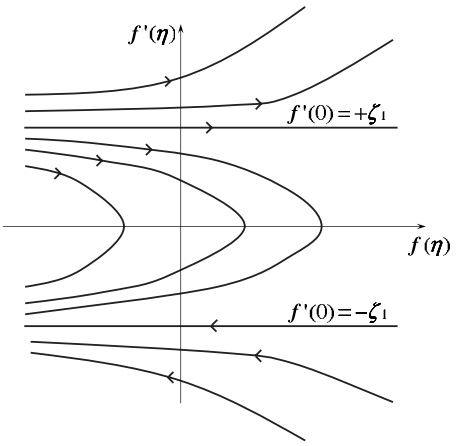

FIG. 2. Sketch of the phase diagram of the reduced similarity equation at small Pr.

$$M = -\frac{\mu_o \chi_\infty \beta_\infty H_0^2}{2\rho_\infty}(\phi+1), \quad \phi \neq -1,$$

$$M = -\frac{\mu_o \chi_\infty \beta_\infty H^2(x_{min})}{2\rho_\infty}, \quad \phi = -1.$$

III. ASYMPTOTIC SOLUTION FOR SMALL PRANDTL NUMBERS

We will now investigate the possibility of deriving an asymptotic solution for the limiting case of small Prandtl numbers (Pr). When $\mathrm{Pr} \ll 1$, viscous effects are negligible. Furthermore, for the purpose of an asymptotic solution, it would suffice to use the average value of the buoyancy force based on an assumed temperature distribution in the similarity equation for the momentum [35]. Thus, considering an approximate quadratic temperature distribution profile [35] would provide the average temperature field as $\bar{\theta}=2/3$. Using this value, considering negligible viscous effects ($f''' \approx 0$), and retaining the rest of the terms in the similarity equation for velocity field [Eq. (25)], we get $(\phi+3)ff''-2(\phi+1)(f')^2+1/3=0$. With standard substitution $f'=p(f)$, we have $f''=p_f(f)f'=p_f p$ from which one finds

$$(\phi+3)fpp_f - 2(\phi+1)p^2 + 1/3 = 0.$$

The latter equation yields

$$(f')^2 = \zeta_1^2 + C\exp\left[4\frac{\phi+1}{\phi+3}f\right], \quad \zeta_1 = \frac{1}{\sqrt{6(\phi+1)}}, \quad (28)$$

where C is the integration constant.

Solution to this equation can be qualitatively analyzed with the following sketch of the phase diagram (see Fig. 2).

It is immediately clear from this figure that solutions with $|f'(0)| > \zeta_1$ grow exponentially, which is not admitted. Furthermore, remarkably, all $|f'(0)| \leq \zeta_1$ are admitted and corresponding solutions tend to $f'=-\zeta_1$ for any initial conditions except for $f'(0)=+\zeta_1$. Thus, mathematically, $f'(0)=\pm\zeta_1$ is possible. However, from a physical point of view, since f' represents the velocity component along the direction parallel to the melt interface, a negative value would imply reverse flow. Thus, $f'(0)=+\zeta_1$ is a physically relevant choice. Furthermore, when $\mathrm{Pr} \ll 1$, the velocity field generally exhibits pluglike profile and variations across the fluid layer are generally weak [35,34]. In consequence, to a good approximation we can set $C=0$ in Eq. (28) and integrate it using the coupled interface boundary condition $B\theta'(0)+(\phi+3)\mathrm{Pr}f(0)=0$ given in Eq. (27). This yields the asymptotic solution for the velocity field as

$$f(\eta) = \zeta_1 \eta + f(0), \quad f(0) = -\frac{B\theta'(0)}{(\phi+3)\mathrm{Pr}},$$

where $\theta'(0)$ is as yet unknown and ζ_1 is given in Eq. (28). It may be noted that using $C=0$ in the above is tantamount to considering $ff''=0$, which has been previously employed in determining asymptotic behavior of boundary layer equations [35]. Furthermore, notice that at $\mathrm{Pr} \ll 1$, as the order of the equations is reduced, the boundary condition $f'(0)=0$ (i.e., no-slip condition) is not applicable anymore as the fluid behaves essentially as an inviscid fluid.

It follows that the expressions for the components of the velocity field can be simplified for this case as

$$\frac{u(x,y)}{U_o} = \zeta_1, \quad \frac{v(x,0)}{U_o} = \frac{B}{4}\left(\frac{\mathrm{Gr}_{M,x}}{4}\right)^{-\phi/4} x^{-\phi/4}\frac{\theta'(0)}{\mathrm{Pr}}.$$

This shows that in particular when $\mathrm{Pr} \ll 1$, the following scaling hold: $u \sim (\phi+1)^{-1/2}$ for the component parallel to the substrate and $v(x,0) \sim \frac{B\theta'(0)}{\mathrm{Pr}}$ for the melting rate at the interface. That is, the melting parameter and the heat transfer rates directly control the rate of substrate melting, while Pr has an inverse relationship with melting rate. The solution can be completed by substituting this similarity equation for the velocity field into that for the original energy equation for the melt [Eq. (26)], which upon integrating and further simplification yields

$$\theta(\eta) = \frac{\mathrm{erf}\{\zeta_2[\zeta_1\eta + f(0)]\} - \mathrm{erf}[\zeta_2 f(0)]}{\{1-\mathrm{erf}[\zeta_2 f(0)]\}}, \quad \zeta_2 = \sqrt{\frac{(\phi+3)\mathrm{Pr}}{2\zeta_1}},$$

where "erf" is the standard error function. Finally, the heat transfer rate at the melt interface can be obtained from this equation as

$$\theta'(0) = \frac{2\zeta_1\zeta_2}{\sqrt{\pi}}\frac{\exp\left[-\left(\frac{\zeta_2 B\theta'(0)}{(\phi+3)\mathrm{Pr}}\right)^2\right]}{\left\{1-\mathrm{erf}\left[-\frac{\zeta_2 B\theta'(0)}{(\phi+3)\mathrm{Pr}}\right]\right\}},$$

which provides a closed-form nonlinear transcendental equation for $\theta'(0)$ in terms of all the governing parameters. For dry substrates, i.e., no melting ($B=0$), the heat transfer rate due to magnetothermal free convection at small Pr reduces to the following simple form:

$$\theta'(0) = \sqrt{\frac{2(\phi+3)\mathrm{Pr}}{\pi\sqrt{6(\phi+1)}}}.$$

IV. NUMERICAL SOLUTION OF SIMILARITY EQUATIONS

The similarity transformation has resulted in two coupled nonlinear ordinary differential equations (ODEs) [Eqs. (25) and (26)] along with boundary conditions, one of which is coupled [Eq. (27)]. However, these ODEs represent a boundary-value problem and not an initial value problem due to the boundary conditions at $\eta=\infty$. The standard approach to solving nonlinear ODEs is to apply one of the many ODE integrators such as Runge-Kutta method [36,37]. These methods work very well when a purely initial value problem is considered; however, when a boundary value problem is undertaken they require guess values on certain unknown quantities such as $f''(0)$, which are then iterated until the boundary condition at $\eta=\infty$ is satisfied leading to the so-called shooting method. Rather than to adopt this approach, we have chosen to apply what is known as an iterative boundary-value technique, which is essentially a nonlinear finite difference method, where the finite difference equations are solved using a pseudo-Newton method. We have chosen this technique for the following two reasons. First, intelligent iteration of the initial conditions in shooting methods requires the computation of sensitivity derivatives [38] which turns what would have been 5 first-order equations into 15 first-order equations. Second and perhaps more important, the shooting methods are not very robust methods and often subject to numerical instability. In particular, it will fail for guess values of the unknown initial conditions that are only a few percent off from the true value of the unknown initial conditions. The iterative boundary-value technique suffers from no such shortcomings as the boundary values are specified entirely within the scheme.

Discretization and numerical solution

The coupled nonlinear ODEs given in Eqs. (25) and (26) are discretized using standard finite difference formulas on a nonequally spaced one-dimensional grid. In this case the grid has a small amount of geometric stretching to cluster points near the melting front ($\eta=0$). The method is derived as follows: let

$$f' = g, \tag{29}$$

which allows one to rewrite Eq. (25) in terms of g

$$g'' + (\phi+3)fg' - 2(\phi+1)g^2 - (\theta-1) = 0,$$

$$\theta'' + (\phi+3)\mathrm{Pr}f\theta' = 0,$$

$$f = \int g d\eta = \int_0^\eta g d\eta + f(0). \tag{30}$$

The domain $\eta \in [0,\infty)$ is split into $JD-1$ (where JD is the number of nodes) nonoverlapping cells with the data stored at the nodes which are denoted by the index j. The equations are discretized using second-order accurate central difference formulas. The central difference formulas for the first and second derivatives are

$$g'' = \left[\frac{g_{j+1}-g_j}{\Delta\eta_{j+1}} - \frac{g_j-g_{j-1}}{\Delta\eta_j}\right]\frac{2}{\Delta\eta_{j+1}+\Delta\eta_j} + O(\Delta\eta^2),$$

$$g' = \frac{g_{j+1}-g_{j-1}}{\Delta\eta_{j+1}+\Delta\eta_j} + O(\Delta\eta^2),$$

$$\Delta\eta_j = \eta_j - \eta_{j-1}. \tag{31}$$

The discretized similarity equations become

$$\left[\frac{g_{j+1}-g_j}{\Delta\eta_{j+1}} - \frac{g_j-g_{j-1}}{\Delta\eta_j}\right]\frac{2}{\Delta\eta_{j+1}+\Delta\eta_j} + (\phi+3)f_j\frac{g_{j+1}-g_{j-1}}{\Delta\eta_{j+1}+\Delta\eta_j} - 2(\phi+1)g_j^2 - (\theta_j-1) = 0,$$

$$\left[\frac{\theta_{j+1}-\theta_j}{\Delta\eta_{j+1}} - \frac{\theta_j-\theta_{j-1}}{\Delta\eta_j}\right]\frac{2}{\Delta\eta_{j+1}+\Delta\eta_j} + (\phi+3)\mathrm{Pr}f_j\frac{\theta_{j+1}-\theta_{j-1}}{\Delta\eta_{j+1}+\Delta\eta_j} = 0, \tag{32}$$

with the coupled boundary condition given as

$$B\left(\frac{-\theta_3+4\theta_2-3\theta_1}{\eta_3-\eta_2+\eta_2-\eta_1}\right) + (\phi+3)\mathrm{Pr}f_1 = 0, \tag{33}$$

which uses a second-order forward difference formula. The values of f at the grid points are computed using the trapezoid rule for the integral defining f as a function of g,

$$\int_0^\eta g d\eta = \sum_{i=2}^{j}\frac{\eta_i-\eta_{i-1}}{2}(g_j+g_{j-1}) + O(\Delta\eta^2). \tag{34}$$

These equations are solved using a pseudo-Newton method. It is not a full Newton method because the values of f_j are not linearized but are treated explicitly. This linearization results in a block tridiagonal matrix which can be inverted exactly using the block variant of the Thomas algorithm [39]. The system of difference equations given in Eq. (32) can be written as

$$\mathbf{R}(\mathbf{q}) = 0,$$

$$\mathbf{q} = (g,\theta)^\dagger, \tag{35}$$

where $\mathbf{R}(\mathbf{q})$ is known as the discrete nonlinear residual and $\mathbf{q}$ is the vector of unknowns over all the grid points j. In order to solve this a pseudo-Newton method is used. A full Newton scheme would be given as

$$\left[\frac{\partial\mathbf{R}(\mathbf{q}^k)}{\partial\mathbf{q}^k}\right]\delta\mathbf{q}^{k+1} = -\mathbf{R}(\mathbf{q}^k),$$

$$\mathbf{q}^{k+1} = \mathbf{q}^k + \delta\mathbf{q}^{k+1}. \tag{36}$$

The pseudo-Newton scheme is given by replacing the exact

linearization of $\mathbf{R}(\mathbf{q})$ by an approximate linearization denoted as $[P]$. The pseudo-Newton scheme is written as

$$[P]\delta\mathbf{q}^{k+1} = -\mathbf{R}(\mathbf{q}^k),$$

$$\mathbf{q}^{k+1} = \mathbf{q}^k + \delta\mathbf{q}^{k+1}. \tag{37}$$

The residual at each point j is known to be a function of quantities at only the grid point j and its nearest neighbors. The particular choice of linearization used in this work allows the linear system given by the pseudo-Newton's method for a point j to be written as

$$[A_j]\delta\mathbf{q}_{j-1} + [D_j]\delta\mathbf{q}_j + [C_j]\delta\mathbf{q}_{j+1} = -\mathbf{R}_j(\mathbf{q}_{j-1}, \mathbf{q}_j^k, \mathbf{q}_{j+1}), \tag{38}$$

where the $[A_j]$, $[D_j]$, and $[D_j]$ define 2×2 block submatrices. The block submatrices are

$$[A_j] = \begin{bmatrix} \dfrac{2}{(\Delta\eta_{j+1}+\Delta\eta_j)\Delta\eta_j} - \dfrac{(\phi+3)f_j}{\Delta\eta_{j+1}+\Delta\eta_j} & 0 \\ 0 & \dfrac{2}{(\Delta\eta_{j+1}+\Delta\eta_j)\Delta\eta_j} - \dfrac{(\phi+3)\mathrm{Pr}f_j}{\Delta\eta_{j+1}+\Delta\eta_j} \end{bmatrix},$$

$$[D_j] = \begin{bmatrix} -\dfrac{2}{\Delta\eta_{j+1}+\Delta\eta_j}\left(\dfrac{1}{\Delta\eta_{j+1}}+\dfrac{1}{\Delta\eta_j}\right) - 4(\phi+1)g_j & 1 \\ 0 & -\dfrac{2}{\Delta\eta_{j+1}+\Delta\eta_j}\left(\dfrac{1}{\Delta\eta_{j+1}}+\dfrac{1}{\Delta\eta_j}\right) \end{bmatrix}, \tag{39}$$

$$[C_j] = \begin{bmatrix} \dfrac{2}{(\Delta\eta_{j+1}+\Delta\eta_j)\Delta\eta_{j+1}} + \dfrac{(\phi+3)f_j}{\Delta\eta_{j+1}+\Delta\eta_j} & 0 \\ 0 & \dfrac{2}{(\Delta\eta_{j+1}+\Delta\eta_j)\Delta\eta_{j+1}} + \dfrac{(\phi+3)\mathrm{Pr}f_j}{\Delta\eta_{j+1}+\Delta\eta_j} \end{bmatrix}.$$

At each Newton step the linear system is inverted exactly and the updates to the state vector are computed. The process continues until the L_2 norm of the residual over the entire mesh is reduced by 12 orders of magnitude from its initial value.

V. RESULTS AND DISCUSSION

The similarity equations have been solved for a set of governing parameters. All solutions were generated using a geometrically stretched grid consisting of 501 nodes with a stretching factor to 1.02. It was found that $\eta_{max}=15.0$ is sufficiently large for the cases considered except for small Prandtl number cases ($\mathrm{Pr}=0.01$) when $\eta_{max}=30.0$ was used. Three different Kelvin force power laws were considered corresponding to $\phi=0.0$, $\phi=1.0$, and $\phi=2.0$ in the magnetic acceleration term by maintaining Prandtl number at $\mathrm{Pr}=10$ and melting parameter at $B=1.0$. Using these set of parameters, the velocity and temperature fields in the melt boundary layer are obtained. Additionally, the effect of variable Prandtl number was considered. Four different Prandtl numbers $\mathrm{Pr}=0.01$, 0.72, 1.0, and 10.0 were considered for Kelvin force with $\phi=1.0$ and a melting parameter of $B=1.0$. The effect of melting parameter was also studied by fixing $\phi=1.0$ and $\mathrm{Pr}=10.0$ and varying $B=0.01$, 0.1, 1.0, and 10.0. For these cases, the normal velocity evaluated at the melting front is also reported. The local normal velocity at the substrate-melt interface has been scaled by its value at $x=L$. That is, the following normalization follows:

$$(\phi+3)f(0)\frac{\dfrac{v(x,0)}{U_o}}{\dfrac{-v(L,0)}{U_o}} = (\phi+3)f(0)\left(\frac{x}{L}\right)^{-(\phi+3)/4}. \tag{40}$$

Furthermore, the local Nusselt number is scaled by its value evaluated at $x=L$, which gives the nondimensional heat transfer rate and is reported by means of the following:

$$\frac{\mathrm{Nu}_x}{\mathrm{Nu}_L} = \theta'(0)\left(\frac{x}{L}\right)^{(\phi+3)/4}. \tag{41}$$

A. Effect of applied magnetic field

In order to analyze the effect of Kelvin force distributions on the solution, power laws correspond to $\phi=0.0$, 1.0, and 2.0 for the Kelvin force with $\mathrm{Pr}=10.0$ and $B=1.0$. It is thought that this represents a plausible physical situation, i.e., a liquid which is readily melted from a solid. A graphical representation of the variation of magnetic field is given in Fig. 3. Note that this is the magnetic-field variation and not the magnetic acceleration or Kelvin force.

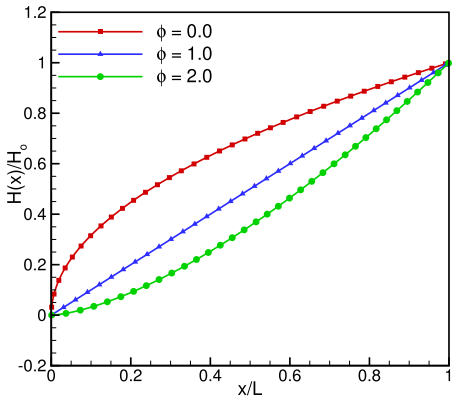

FIG. 3. (Color online) Graphical representation of magnetic field for various values of the power-law exponent of the Kelvin force [ϕ=0.0 (red square), ϕ=1.0 (blue triangle), and ϕ=2.0 (green circle)].

Figures 4(a) and 4(b) show the velocity and temperature profiles in the melt boundary layer for the above parameter range. The scaled velocity normal to the substrate is depicted in Fig. 5. The effect of Kelvin force variation for all quantities is made quite apparent. The highest peak for the profile of velocity component parallel to the substrate is observed for the case with ϕ=0.0 for the Kelvin force while the lowest is observed for ϕ=2.0. Furthermore, the melt boundary layer

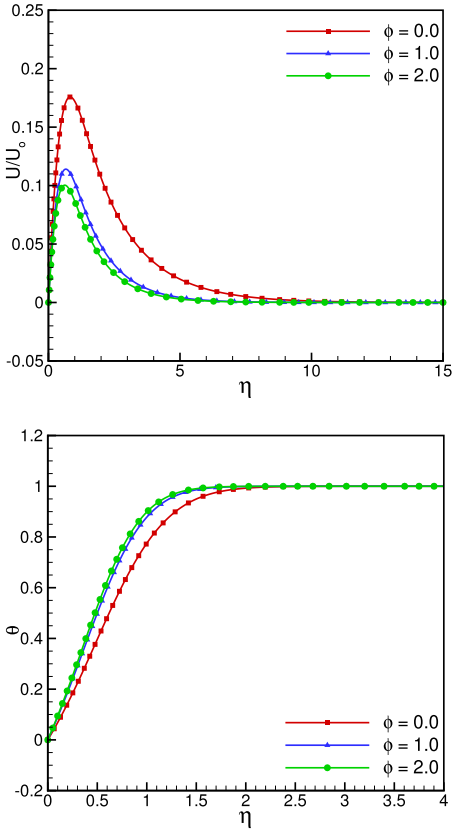

FIG. 4. (Color online) Nondimensional velocity and temperature profiles with Pr=10.0, B=1.0, and various values of the power law exponent of the Kelvin force [ϕ=0.0 (red square), ϕ=1.0 (blue triangle), and ϕ=2.0 (green circle)].

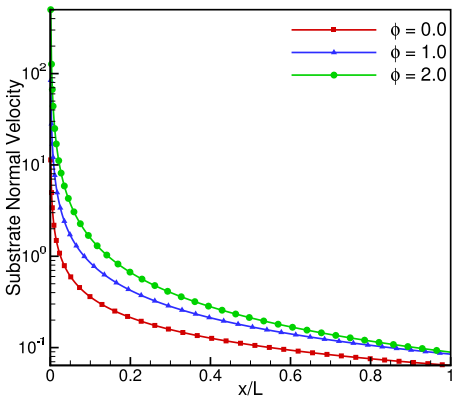

FIG. 5. (Color online) Nondimensional normal velocity at the melting front $-(\phi+3)f(0)\frac{v(x,0)}{v(x,L)}$ [see Eq. (40)] vs axial coordinate $X=x/L$ with Pr=10.0, B=1.0, and various values of the exponent of the Kelvin force [ϕ=0.0 (red square), ϕ=1.0 (blue triangle), and ϕ=2.0 (green circle)].

is also thickest for ϕ=0.0. It is apparent that the thermal boundary layer thickness is affected in a similar way as that of the velocity boundary layer when ϕ is varied. The velocity component normal to the substrate that characterizes the melting rate exhibits an interesting variation with changes in magnetic-field gradients as specified by different ϕ. In particular, substantially higher substrate normal velocities at the melting front are observed with ϕ=2.0 as compared to ϕ=1.0 and 0.0. The effect of magnetic-field gradient on the heat transfer coefficient is shown in Fig. 6. An interesting finding that follows by integrating these curves is that the highest heat transfer is achieved when the power-law exponent ϕ=1.0 is considered for the Kelvin force as shown numerically in Table I.

B. Effect of Prandtl number

An analogous study has been conducted for various Prandtl numbers to assess the effect of material on the melting substrate similarity profiles and heat transfer rates by keeping ϕ=1.0 and B=1.0. Figures 7(a) and 7(b) show the

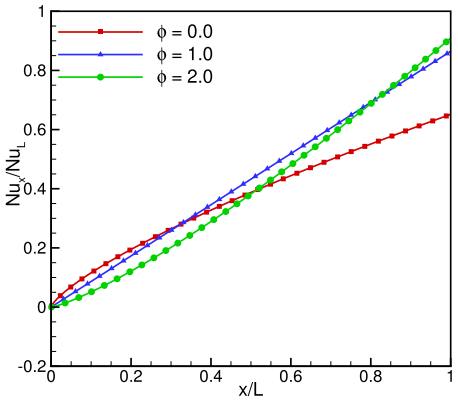

FIG. 6. (Color online) Nondimensional heat transfer coefficient $\mathrm{Nu}_x/\mathrm{Nu}_L$ vs axial coordinate x/L with Pr=10.0, B=1.0, and various values of the exponent of the Kelvin force [ϕ=0.0 (red square), ϕ=1.0 (blue triangle), and ϕ=2.0 (green circle)].

TABLE I. Nondimensional total heat transfer rates with various values of the power law exponent for the Kelvin force.

ϕ	$\int_{x/L=0}^{x/L=1}\theta'(0)\frac{\mathrm{Nu}_x}{\mathrm{Nu}_L}d(\frac{x}{L})$
0.0	0.3729
1.0	0.4332
2.0	0.4049

resulting similarity velocity and temperature profiles in the melt.

As with the variation of Kelvin force, the variation of the Prandtl number has significant effects on the velocity boundary layer. In particular, when the Pr is the lowest, it exhibits the highest peak velocity as well as wider distribution within the boundary layer, consistent with classical results available for free convection without Kelvin force or melting [40]. Furthermore, as expected, the thermal boundary layer also becomes the thickest for the lowest Pr. The most interesting effect following as a consequence of this aspect is shown in the normal velocity at the substrate shown in Fig. 8, with the lowest Pr showing the highest magnitude indicating that the substrate melts at substantially larger rates for these parameters.

The effect of Pr on heat transfer rate is depicted in Fig. 9.

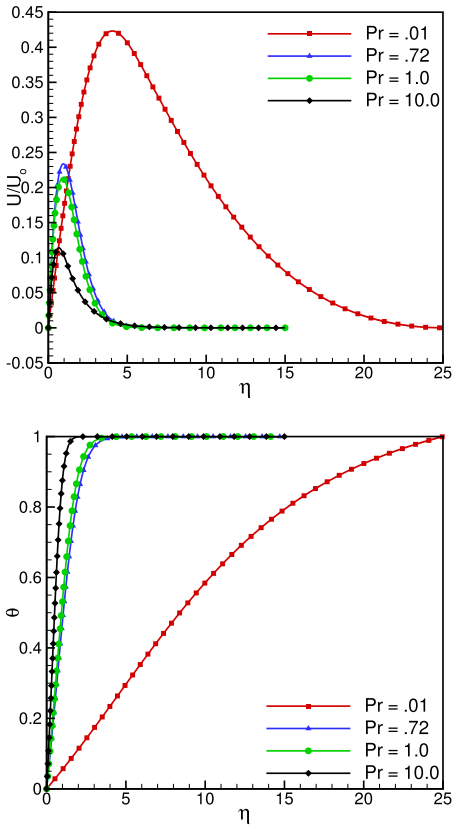

FIG. 7. (Color online) Nondimensional velocity and temperature profiles with $\phi=1.0$, $B=1.0$, and variable Prandtl number [Pr=0.01 (red square), Pr=0.72 (blue triangle), Pr=1.0 (green circle), and Pr=10.0 (black diamond)].

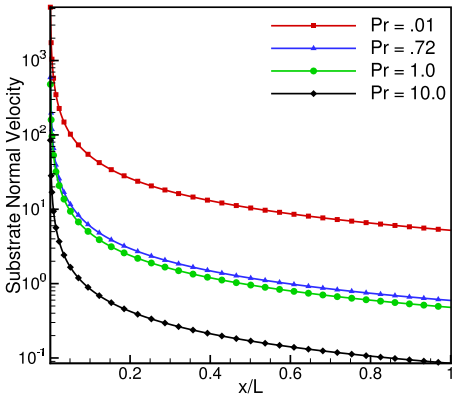

FIG. 8. (Color online) Nondimensional normal velocity at the melting front $-(\phi+3)f(0)\frac{v(x,0)}{v(x,L)}$ [see Eq. (40)] vs axial coordinate $X=x/L$ with $B=1.0$, $\phi=1.0$, and various values of Prandtl number [Pr=0.01 (red square), Pr=0.72 (blue triangle), Pr=1.0 (green circle), and Pr=10.0 (black diamond)].

The higher the Pr, the greater the rate is at which heat is transferred from the fluid to the substrate needed for melting. This follows as a direct result of the nature of the gradient in the temperature profile in the thermal boundary layer as a function of Pr. In particular, for higher Pr, the thermal boundary layer gets thinner and has higher gradients at the melt interface which serve to increase the heat transfer rate to the substrate. Table II contains the values of the nondimensional temperature gradient at the melting front and clearly illustrates the increase in this gradient as a function of the Prandtl number. Thus, for this aspect, the thinning of the thermal boundary layer has the dominant effect when the nature of the fluid or the Pr is changed.

C. Effect of melting rate

The effect of melting parameter on the similarity profile as well as the heat transfer rate was investigated using the following set of values: $B=0.01$, 0.1, 1.0, and 10.0. Again the Kelvin force is specified such that $\phi=1.0$ and Pr=10.0.

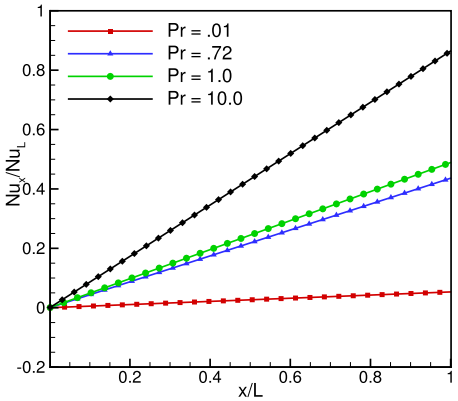

FIG. 9. (Color online) Nondimensional heat transfer coefficient $\mathrm{Nu}_x/\mathrm{Nu}_L$ vs axial coordinate x/L with $B=1.0$, $\phi=1.0$, and various values of Prandtl number [Pr=0.01 (red square), Pr=0.72 (blue triangle), Pr=1.0 (green circle), and Pr=10.0 (black diamond)].

TABLE II. Nondimensional temperature gradient at the melting front as a function of Prandtl number Pr.

Pr	$\theta'(0)$
0.01	0.0532
0.72	0.4362
1.0	0.4889
10.0	0.8646

Figures 10(a) and 10(b) show the similarity velocity and temperature profiles.

The figures make the effect of the melting parameter quite apparent. The velocity parallel to the substrate has a higher peak value for higher values of B. Increasing the melting parameter to $B=10.0$ results in a very dramatic increase in the maximum magnitude of this velocity component as well as the boundary layer thickness. At the interface front, the normal velocity component has the highest magnitude for the highest melting parameter considered as depicted in Fig. 11. This is expected as the melting parameter directly controls the rate at which the substrate recedes. Notice that for both the components of the velocity profiles there is a very large difference between the results for $B=1.0$ and $B=10.0$. In comparison, however, the melting parameter has a mild relative influence on the temperature profile. Since the interface front temperature is fixed, this observation is reasonable. Figure 10(b) shows that generally for higher values of B, the boundary layer tends to thicken, which however reverts at the highest value considered ($B=10.0$) due to the inherent nonlinear effect of the melting parameter on the coupled transport phenomena.

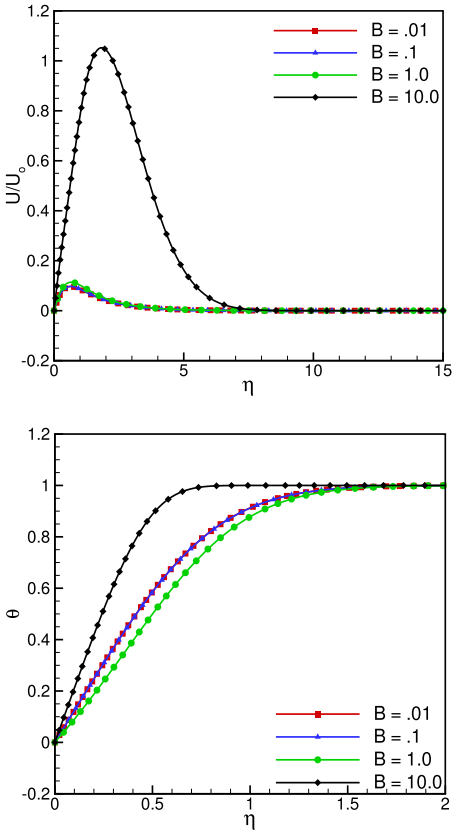

FIG. 10. (Color online) Nondimensional velocity and temperature profiles with $\phi=1.0$, Pr=10.0, and variable melting parameter [$B=0.01$ (red square), $B=0.1$ (blue triangle), $B=1.0$ (green circle), and $B=10.0$ (black diamond)]. Note that red squares and blue triangles overlap.

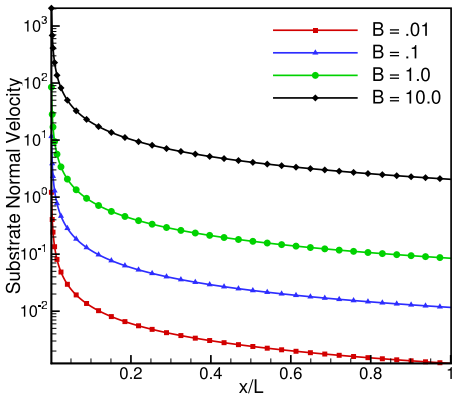

FIG. 11. (Color online) Nondimensional normal velocity at the melting front $-(\phi+3)f(0)\frac{v(x,0)}{v(x,L)}$ [see Eq. (40)] vs axial coordinate $X=x/L$ with $\phi=1.0$, Pr=10.0, and various values of the melting parameter [$B=0.01$ (red square), $B=0.1$ (blue triangle), $B=1.0$ (green circle), and $B=10.0$ (black diamond)].

This nonlinear effect of B is further evident on the heat transfer rates (see Fig. 12). There is hardly any difference between $B=0.01$ and $B=0.1$. However, the contrast between $B=0.1$ and $B=1.0$ is quite staggering and even more staggering is the contrast between $B=1.0$ and $B=10.0$. The heat transfer has actually increased (again in contrast to the trend demonstrated by the results at lower values of B). There is a physical explanation for these phenomena. When the melting rate is increased at higher values of B more material of the substrate melts and joins the fluid, while for lower values of the melting parameter this has the effect of decreasing heat transfer. This is because at lower B, the thermal gradients at the interface front on the fluid side is lower. Furthermore, more of the heat supplied needs to overcome the greater

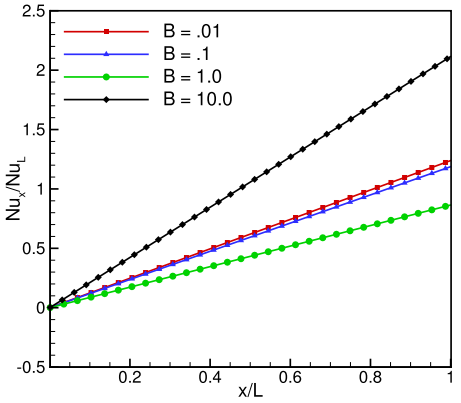

FIG. 12. (Color online) Nondimensional heat transfer coefficient $\mathrm{Nu}_x/\mathrm{Nu}_L$ vs axial coordinate x/L with $\phi=1.0$, Pr=10.0, and various values of the melting parameter [$B=0.01$ (red square), $B=0.1$ (blue triangle), $B=1.0$ (green circle), and $B=10.0$ (black diamond)].

degree of subcooling present in the substrate side, i.e., higher values of the solid phase Stefan number Ste_s as reflected in the definition of B. On the other hand, for $B=10.0$ the substrate is melting so readily that relatively very large magnitudes of melt flow are induced which causes the thermal gradients at the melting front to increase and thus increase the heat transfer.

VI. SUMMARY AND CONCLUSIONS

The magnetothermal free convection of an electrically insulating fluid resulting from the melting of a semi-infinite substrate subjected to thermal and magnetic-field gradients in a microgravity environment is considered. To facilitate analysis, the magnetic-field gradient characterized as the Kelvin force is recast as a buoyancy force with an effective spatially dependent magnetic acceleration term. Similarity solution of the boundary layer transport equations of the melt flow is achieved when such acceleration term is expressed as a power law in terms of the axial coordinate parallel to the substrate. For small Prandtl numbers, when the viscous effects can be neglected, this results in a closed-form asymptotic solution for the velocity and thermal fields in the melt boundary layer as well as the mass and heat transport rate across the substrate. For numerical solution in the general case, an iterative nonlinear boundary-value technique based on a finite-difference formulation proved to be robust and efficient.

The effect of different values of the power-law exponent for the magnetic-field gradient on the structure of the melt flow boundary layer as well as substrate heat and mass transport rates is illustrated for a representative set of parameters. Furthermore, the influence of the nature of the material (Prandtl number) as well as the melting parameter have been considered and analyzed with striking trends shown in each case. Variable magnetic field is one of the most important parameters for this problem as suitable schemes can be devised to appropriately control the mass or energy transport rates across the substrate. For example, for the set of parameters considered ($\phi=0.0$, 1.0, and 2.0), the heat transfer rate to the substrate is maximized if the Kelvin force with the exponent $\phi=1.0$ is used. Furthermore, the melting parameter has a profound influence on the behavior of this nonlinear coupled transport problem. For example, if the substrate is melted such that the value of B is relatively moderate, then the heat transfer rate to the substrate is correspondingly relatively low. On the other hand, if higher values of B is employed, then a large amount of material is melted from the substrate that joins the fluid causing pronounced magnetic gradient induced free convection and heat transfer rates. While the results reported here are representative for this problem providing basic insights, the approach reported provides a convenient theoretical and computational setting for analysis of phase-change problems driven by thermal and magnetic-field gradients in microgravity environments.

[1] R. Rosensweig, *Ferrohydrodynamics* (Dover Publications, New York, 1997).
[2] R. Moreau, *Magnetohydrodynamics* (Springer, New York, 1990).
[3] D. Gray, J. Huang, and B. Edwards, Int. J. Eng. Sci. **39**, 1837 (2001).
[4] E. Beaugnon and R. Tournier, Nature (London) **349**, 470 (1991).
[5] D. Braithwaite, E. Beaugnon, and R. Tournier, Nature (London) **354**, 134 (1991).
[6] J. Carruthers and R. Wolfe, J. Appl. Phys. **39**, 5718 (1968).
[7] D. Clark and W. Honeywell, AIChE J. **23**, 553 (1977).
[8] J. Huang, B. Edwards, and D. Gray, Phys. Fluids **9**, 1819 (1997).
[9] J. Huang, B. F. Edwards, and D. D. Gray, Phys. Rev. E **57**, R29 (1998).
[10] J. Huang, D. D. Gray, and B. F. Edwards, Phys. Rev. E **57**, 5564 (1998).
[11] J. Huang, D. D. Gray, and B. F. Edwards, Phys. Rev. E **58**, 5164 (1998).
[12] B. Finlayson, J. Fluid Mech. **40**, 753 (1970).
[13] R. Ganguly, S. Sen, and I. Puri, Phys. Fluids **16**, 2228 (2004).
[14] A. Mukhopadhyay, R. Ganguly, S. Sen, and I. Puri, Int. J. Heat Mass Transfer **48**, 3485 (2005).
[15] B. Bai, A. Yabe, and J. Qi, AIAA J. **37**, 1538 (1999).
[16] N. Wakayama, C. Zhong, T. Kiyoshi, K. Itoh, and H. Wada, AIChE J. **47**, 2640 (2001).
[17] M. Akamatsu, M. Higano, and H. Ogasawara, Ann. N.Y. Acad. Sci. **1077**, 613 (2006).
[18] T. Bednarz, J. Patterson, C. Lei, and H. Ozoe, Int. Commun. Heat Mass Transfer **36**, 781 (2009).
[19] F. Larachi and M. Munteanu, Ind. Eng. Chem. Res. **49**, 3623 (2010).
[20] M. Schieber, J. Cryst. Growth **1**, 131 (1967).
[21] N. Wakayama, M. Ataka, and H. Abe, J. Cryst. Growth **178**, 653 (1997).
[22] S. Lin, M. Zhou, A. Azzi, J. Xu, N. Wakayama, and A. Ataka, Biochem. Biophys. Res. Commun. **275**, 274 (2000).
[23] M. Tagami, M. Hamai, I. Mogi, K. Watanbe, and M. Motokawa, J. Cryst. Growth **203**, 594 (1999).
[24] N. Ramachandran and F. Leslie, J. Cryst. Growth **274**, 297 (2005).
[25] L. Rubinstein, *The Stefan Problem* (American Mathematical Society, Providence, RI, 1994).
[26] G. Oreper and J. Szekely, J. Cryst. Growth **64**, 505 (1983).
[27] R. Series and D. Hurle, J. Cryst. Growth **113**, 305 (1991).
[28] P. Davidson, Annu. Rev. Fluid Mech. **31**, 273 (1998).
[29] R. Seeniraj and N. Kannan, Int. J. Heat Mass Transfer **46**, 1599 (2003).
[30] W. Deen, *Analysis of Transport Phenomena* (Oxford University Press, New York, 1998).
[31] H. Landau, Q. Appl. Math. **8**, 81 (1950).
[32] L. Roberts, J. Fluid Mech. **4**, 505 (1958).
[33] Y. Yen and C. Tien, J. Geophys. Res. **68**, 3673 (1963).

[34] M. Epstein and D. Cho, ASME J. Heat Transfer **98**, 531 (1976).
[35] P. Lykoudis, Int. J. Heat Mass Transfer **5**, 23 (1962).
[36] J. Butcher, *Numerical Methods for Ordinary Differential Equations* (Wiley, West Sussex, England, 2008).
[37] J. Lambert, *Numerical Methods for Ordinary Differential Equations: The Initial Value Problem* (Wiley, West Sussex, England, 1991).
[38] K. Milan and V. Hlavacek, *Numerical Solution of Nonlinear Boundary Value Problems with Applications* (Prentice-Hall, New Jersey, 1983).
[39] J. Thomas, *Numerical Partial Differential Equations: Finite Difference Methods* (Springer, New York, 1995).
[40] S. Ostrach, NACA Technical Note Report No. 1111, 1953 (unpublished).